Journal of Alloys and Compounds 772 (2019) 593–602

Contents lists available at ScienceDirect

Journal of Alloys and Compounds

journal homepage: http://www.elsevier.com/locate/jalcom

Clarification of electronic and thermal transport properties of Pb-, Ag-, and Cu-doped p-type $Bi_{0.52}Sb_{1.48}Te_3$

Kwanlae Kim [a, b], Gwansik Kim [a], Sang Il Kim [c], Kyu Hyoung Lee [a, **], Wooyoung Lee [a, *]

[a] Department of Materials Science and Engineering, Yonsei University, Seoul 03722, South Korea
[b] Department of Manufacturing Systems and Design Engineering, Seoul National University of Science and Technology (SeoulTech), Seoul 01811, South Korea
[c] Department of Materials Science and Engineering, University of Seoul, Seoul 02504, South Korea

ARTICLE INFO

Article history:
Received 24 July 2018
Received in revised form
5 September 2018
Accepted 10 September 2018
Available online 11 September 2018

Keywords:
Bi_2Te_3
Thermoelectric power generation
Doping
Transport parameter
Bipolar conduction

ABSTRACT

The feasibility of using Bi_2Te_3-based alloys in low-grade heat thermoelectric power generation has been intensively investigated via a substitutional doping approach over the last decade. However, the comprehensive and quantitative understanding of the electronic and thermal transport parameters of doped Bi_2Te_3-based alloys including their carrier concentration (n_c), carrier mobility (μ_{Hall}), density of state (DOS) effective mass (m_d^*), and electronic (κ_{ele}), lattice (κ_{lat}), and bipolar thermal (κ_{bp}) conductivities is still elusive. The understanding of these parameters is a prerequisite for designing the modules for real-time applications. In this study, we investigated the effect of Pb, Ag, and Cu doping on the thermoelectric transport parameters of *p*-type $Bi_{0.52}Sb_{1.48}Te_3$ (BST) both theoretically and experimentally. The thermoelectric transport properties of BST and their temperature dependences could be systematically tuned in a low-temperature range by controlled doping of Pb, Ag, and Cu mainly because of the increased concentration of the majority hole carriers. In addition, a zT value of 1 could be obtained over the wide temperature range of 300–400 K by optimizing the doping elements and contents because of the synergetic effect of the suppression of bipolar conduction at higher temperatures and the gradual increase in m_d^* with the doping content at $n_c < 10^{20}$ cm^{-3}.

1. Introduction

Owing to the increasing demand for environmental-friendly energy sources with zero carbon emission, thermoelectric power generation (TEG) has gained immense attention over the past few years [1,2]. In particular, TEG offers several advantages such as soundless operation and scalability over other power generation system. It has been estimated that approximately 78% of waste heat energy (mainly those associated with manufacturing, transportation, and power plants) is released in the low-temperature range (<200 °C) [3]. Hence, intensive research has been carried out for the development of high TE performance Bi_2Te_3-based alloys to enable a highly-efficient TEG at low temperatures [4–8].

The TE energy conversion efficiency of a material is evaluated by its zT value, which is a dimensionless figure of merit and is given by $zT = \sigma S^2 T/\kappa_{tot}$, where σ is the electrical conductivity, S is the Seebeck coefficient, and κ_{tot} is the total thermal conductivity at a given absolute temperature T [9]. Bi-Sb-Te ternary compounds are the most commonly used *p*-type Bi_2Te_3-based TE materials because of their high zT value (~1.0) at 300 K [10]. However, to utilize the waste-heat sources effectively over the entire low-temperature range of 300–450 K, it is imperative to adjust the temperature so as to obtain the maximum zT value (zT_{max}). In undoped Bi-Sb-Te alloys, $zT \neq zT_{max}$ at temperatures higher than 320 K. This is because at higher temperatures, κ_{bp} starts increasing, which in turn increases κ_{tot}. Thus, substitutional doping, which generates additional hole carriers, is an effective approach to decrease the contribution of κ_{bp}. It can also improve the TE transport properties of Bi-Sb-Te systems because of the increased DOS near the Fermi level due to band modification [11] and intensified phonon scattering due to the formation of point defects [5]. Various studies have been carried out to investigate the effect of doping elements such as Pb [12–14], Ag [15–17], and Cu [18–20] on the TE performance of *p*-type Bi-Sb-Te systems. It has been found that the doping of all these elements in BST systems suppresses their κ_{bp}, which increases the temperature required to reach zT_{max}. However, very little information is available on the temperature dependence of the physical parameters of these systems such as n_c, μ_{Hall}, m_d^*, κ_{ele},

* Corresponding author.
** Corresponding author.
E-mail addresses: khlee2018@yonsei.ac.kr (K.H. Lee), wooyoung@yonsei.ac.kr (W. Lee).

https://doi.org/10.1016/j.jallcom.2018.09.099
0925-8388/

κ_{lat}, and κ_{bp}, which determine their TE transport properties. Therefore, the experimental and theoretical investigations of the effect of doping on the physical parameters of BST systems would provide a stereoscopic understanding of their carrier and phonon transports, ultimately providing the guidelines for optimum material design for TEG applications.

In this study, we investigated the effect of doping and temperature dependence of the electronic and thermal transport properties of Bi-Sb-Te ternary compounds. We used systematically designed Pb-, Ag-, and Cu-doped BST polycrystalline bulks with the n_c range of 1.8×10^{19}–9.69×10^{19} cm^{-3}. The temperature dependence of the electronic transport properties could be tuned by controlling the value of n_c. In addition, the temperature-dependent thermal conduction of the samples was elucidated based on the single parabolic band (SPB) [21] and Callaway models [22].

2. Experimental method

High purity (>99.99%) Bi, Sb, Te, Pb, Ag, and Cu granules were weighed according to the composition $Bi_{0.52}Sb_{1.48-x}M_xTe_3$ ($x = 0$–0.01(0–0.5 at.%), M = Pb, Ag, Cu) and were loaded into vacuum-sealed quartz tubes (14 mm diameter) at 10^{-4} Torr. The ingots were prepared via a melt-solidification process, and melting was carried out in a box furnace for 10 h at 1085 °C. The resulting ingots were crushed into powders using a pestle mortar. The crushed powders were sieved to obtain particles smaller than 53 μm. Then, disk-shaped compacted polycrystalline bulk samples were prepared by using the spark plasma sintering (SPS) technique at 45 MPa and 480 °C for 3 min in vacuum. In order to measure σ, S, and κ in the same direction, bar-shaped samples (3 mm × 3 mm × 10 mm) for σ and S measurements and square-shaped samples (10 mm × 10 mm × 1.5 mm) for thermal diffusivity measurement were cut on a plane parallel and perpendicular to the SPS press direction, respectively.

The phases of the sintered samples were analyzed using X-ray diffraction (XRD) (Ultima IV/ME 200DX, Rigaku, Japan) with CuKα radiation. The microstructures of the fractured surfaces were analyzed using field emission scanning electron microscopy (SEM) (JEOL-7800F). To estimate the n_c and μ_{Hall} of the samples, Hall effect measurements were carried out in the van der Pauw configuration in the presence of a magnetic field of 1 T. The n_c and μ_{Hall} values were then computed using the one-band model. The temperature dependence of σ and S (300–520 K) was investigated using a thermoelectric property measurement system (ZEM-3, ULVAC, Japan). The value of κ_{tot} was calculated using the relation $\kappa_{tot} = \rho_s C_p \lambda$, where ρ_s is the density, C_p is the heat capacity, and λ is the thermal diffusivity of the BST samples. The laser flash method (Netzsch LFA-457, Germany) was used to measure the temperature dependence of λ. C_p for the low-temperature range (100–400 K) was measured using a quantum design physical properties measurement system. The measured C_p values (at $T > 270$ K) were almost the same (~0.186 J g^{-1} K^{-1}) for all the samples. Therefore, in this study, the value of C_p was taken to be 0.186 J g^{-1} K^{-1} over the temperature range of 300–520 K. The measured ρ_s for the sintered samples was ~6.65 g cm^{-3}.

3. Results and discussion

3.1. Phase and structure analyses

The electronic and thermal transport properties of Bi_2Te_3-based alloys are significantly influenced by their structural characteristics (*e.g.* grain size and crystal orientation) as well as composition. Thus, prior to discussing the TE transport properties of the Pb-, Ag-, and Cu-doped BST alloys investigated in this study, the analyses of their phase and structure were carried out by XRD and SEM. Fig. 1(a)–(c) show the XRD profiles of the planes perpendicular to the SPS pressing direction of the sintered $Bi_{0.52}Sb_{1.48-x}M_xTe_3$ samples. All major peaks could be indexed to the rhombohedral Sb_2Te_3 structure (space group: $R\bar{3}m$). The sintered samples showed no secondary phase, indicating that most of the Pb, Ag, and Cu atoms substituted into the Bi/Sb sites. The XRD patterns and SEM images of the fractured surfaces of the samples (Fig. 1(d)) revealed that Pb, Ag, and Cu doping did not affect their microstructural evolution during the SPS process significantly. The texture fraction (f_{00l}) values for the {0 0 l} planes of the Pb-, Ag-, and Cu-doped BST samples were computed using the Lotgering method [23]. The samples showed f_{00l} values in the range of 0.21–0.31, and the average grain size of the samples was ~10 μm. This confirms that BST samples with controlled structures and compositions were successfully prepared.

The lattice parameters a and c increased to 4.3000 Å and 30.5240 Å by a 0.25 at.% Pb incorporation and 4.3029 Å and 30.5483 Å by a 0.5 at.% Pb incorporation from 4.2996 Å and 30.5111 Å (Pristine BST), respectively [14]. This is because Pb with a 180 pm atomic radius was substituted to Bi (160 pm)/Sb (145 pm) sites. A substitutional doping of Pb into Bi/Sb sites generating holes can be also confirmed from the increased n_c in Table 1. Contrarily, lattice parameters a and c did not noticeably increase or decrease by incorporating Ag or Cu because of the similar atomic radius between Ag (160 pm)/Cu (135 pm) and Bi/Sb. Nevertheless, the substitutional doping of Ag/Cu into Bi/Sb sites can be identified from the gradual increase of n_c by incorporating Ag or Cu (Table 1).

3.2. Electronic transport properties

The electronic transport properties of the samples were investigated by analyzing the temperature dependence of their σ, S, and power factor (σS^2). As shown in Fig. 2, the doping effect of Pb, Ag, Cu on BST is clearly observed from σ and S values as a function of temperature. The σ of BST is increased by doping of Pb, Ag, and Cu, suggesting that the hole carriers were generated by the substitution of these doping elements at the Bi/Sb sites (Figs. 2(a)–(c)). In addition, for the same doping level, the Ag-doped sample showed a much higher increase in the σ value than the Pb- and Cu-doped samples. At 300 K and a doping content of 0.5 at.%, the σ value of the Ag-doped BST sample was found to be about 3.3×10^5 Sm^{-1}, while those of the Pb- and Cu-doped BST samples were lower than 2.0×10^5 Sm^{-1}. At 300 K, the S of the Pb-, Ag-, and Cu-doped BST exhibited a trade-off relationship with σ, as shown in Figs. 2(d)–(f). It can be observed that the S_{max} temperature shifted toward higher temperatures with an increase in the doping content mainly because of the suppressed bipolar conduction. The mechanism for the suppression of κ_{bp} will be discussed later. Fig. 2(g)–(i) show the temperature dependence of the power factor values of the $Bi_{0.52}Sb_{1.48-x}M_xTe_3$ samples. It was found that at an optimum doping content, the samples showed the maximum power factor at 300 K. The optimum Pb (4.31 mW m^{-1} K^{-2}), Ag (4.20 mW m^{-1} K^{-2}), and Cu (4.42 mW m^{-1} K^{-2}) contents were found to be 0.38, 0.13, and 0.13 at.%, respectively. Unlike the case at 300 K, the power factor of the samples did not decrease with an increase in the doping contents at 520 K.

Since the electronic transport properties of BST systems strongly depend on their physical parameters such as n_c and μ_{Hall}, we estimated these parameters at 300 and 520 K by carrying out Hall measurements. The results are shown in Table 1 and Fig. 3. At both 300 and 520 K, n_c increased with an increase in the doping content, suggesting that Pb, Ag, and Cu are effective acceptors for p-type BST systems. At 300 K, the σ values of the $Bi_{0.52}Sb_{1.48-x}M_xTe_3$ samples

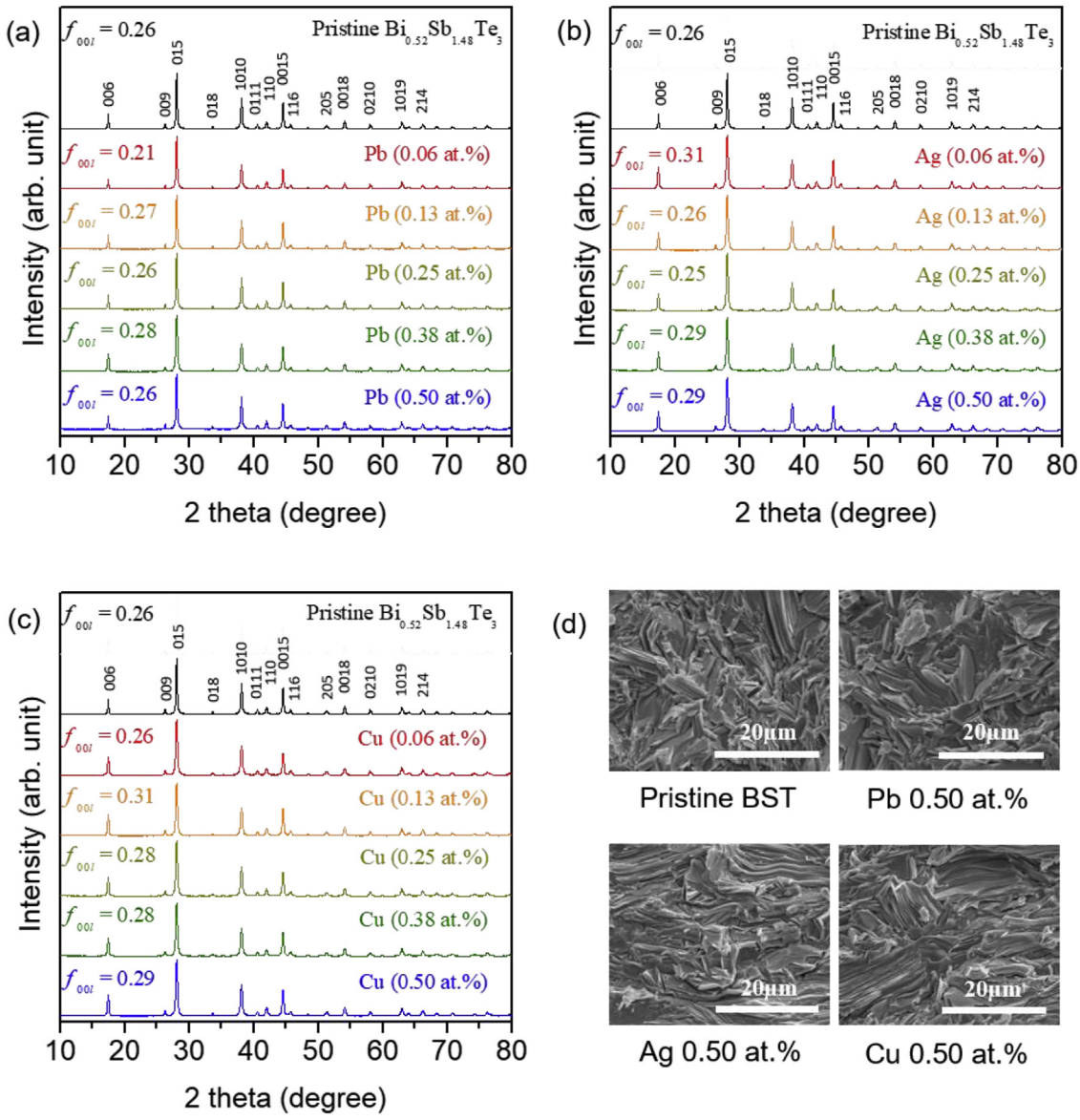

Fig. 1. XRD patterns of the $Bi_{0.52}Sb_{1.48-x}M_xTe_3$ ($x = 0–0.01(0.5$ at.%)) sintered bulk samples, where M is (a) Pb, (b) Ag, and (c) Cu. (d) SEM images of the fractured surfaces of pristine BST and the Pb 0.50 at.%, Ag 0.50 at.%, and Cu 0.50 at.% BST samples. The XRD data for Pb doping were taken from Ref. [14].

Table 1
Carrier concentration (n_c) and carrier mobility (μ_{Hall}) of $Bi_{0.52}Sb_{1.48-x}M_xTe_3$ ($x = 0–0.01(0.5$ at.%)), where M is Pb, Ag, and Cu at 300 and 520 K. The data for Pb doping at 300 K were taken from Ref. [14].

	n_c(300 K) (cm^{-3})	μ_{Hall} (300 K) ($cm^2 V^{-1}s^{-1}$)	n_c(520 K) (cm^{-3})	μ_{Hall} (520 K) ($cm^2 V^{-1}s^{-1}$)
$Bi_{0.52}Sb_{1.48}Te_3$	1.80×10^{19}	236.4	3.57×10^{19}	70.9
$Bi_{0.52}Sb_{1.47875}Pb_{0.00125}Te_3$	2.23×10^{19}	229.7	3.53×10^{19}	72.2
$Bi_{0.52}Sb_{1.4775}Pb_{0.0025}Te_3$	2.65×10^{19}	223.9	3.74×10^{19}	71.3
$Bi_{0.52}Sb_{1.475}Pb_{0.005}Te_3$	3.71×10^{19}	235.5	4.18×10^{19}	83.9
$Bi_{0.52}Sb_{1.4725}Pb_{0.0075}Te_3$	4.78×10^{19}	229.8	4.88×10^{19}	85.0
$Bi_{0.52}Sb_{1.47}Pb_{0.01}Te_3$	6.29×10^{19}	198.4	6.43×10^{19}	71.9
$Bi_{0.52}Sb_{1.47875}Ag_{0.00125}Te_3$	2.41×10^{19}	232.3	3.73×10^{19}	69.0
$Bi_{0.52}Sb_{1.4775}Ag_{0.0025}Te_3$	3.30×10^{19}	215.7	3.89×10^{19}	77.9
$Bi_{0.52}Sb_{1.475}Ag_{0.005}Te_3$	5.01×10^{19}	236.9	5.22×10^{19}	82.6
$Bi_{0.52}Sb_{1.4725}Ag_{0.0075}Te_3$	6.80×10^{19}	221.5	6.91×10^{19}	82.0
$Bi_{0.52}Sb_{1.47}Ag_{0.01}Te_3$	9.69×10^{19}	213.1	9.80×10^{19}	78.2
$Bi_{0.52}Sb_{1.47875}Cu_{0.00125}Te_3$	2.23×10^{19}	238.8	3.69×10^{19}	67.0
$Bi_{0.52}Sb_{1.4775}Cu_{0.0025}Te_3$	2.76×10^{19}	235.4	3.78×10^{19}	76.7
$Bi_{0.52}Sb_{1.475}Cu_{0.005}Te_3$	3.63×10^{19}	246.9	4.17×10^{19}	82.2
$Bi_{0.52}Sb_{1.4725}Cu_{0.0075}Te_3$	4.42×10^{19}	229.8	4.65×10^{19}	77.6
$Bi_{0.52}Sb_{1.47}Cu_{0.01}Te_3$	5.52×10^{19}	204.0	5.68×10^{19}	70.0

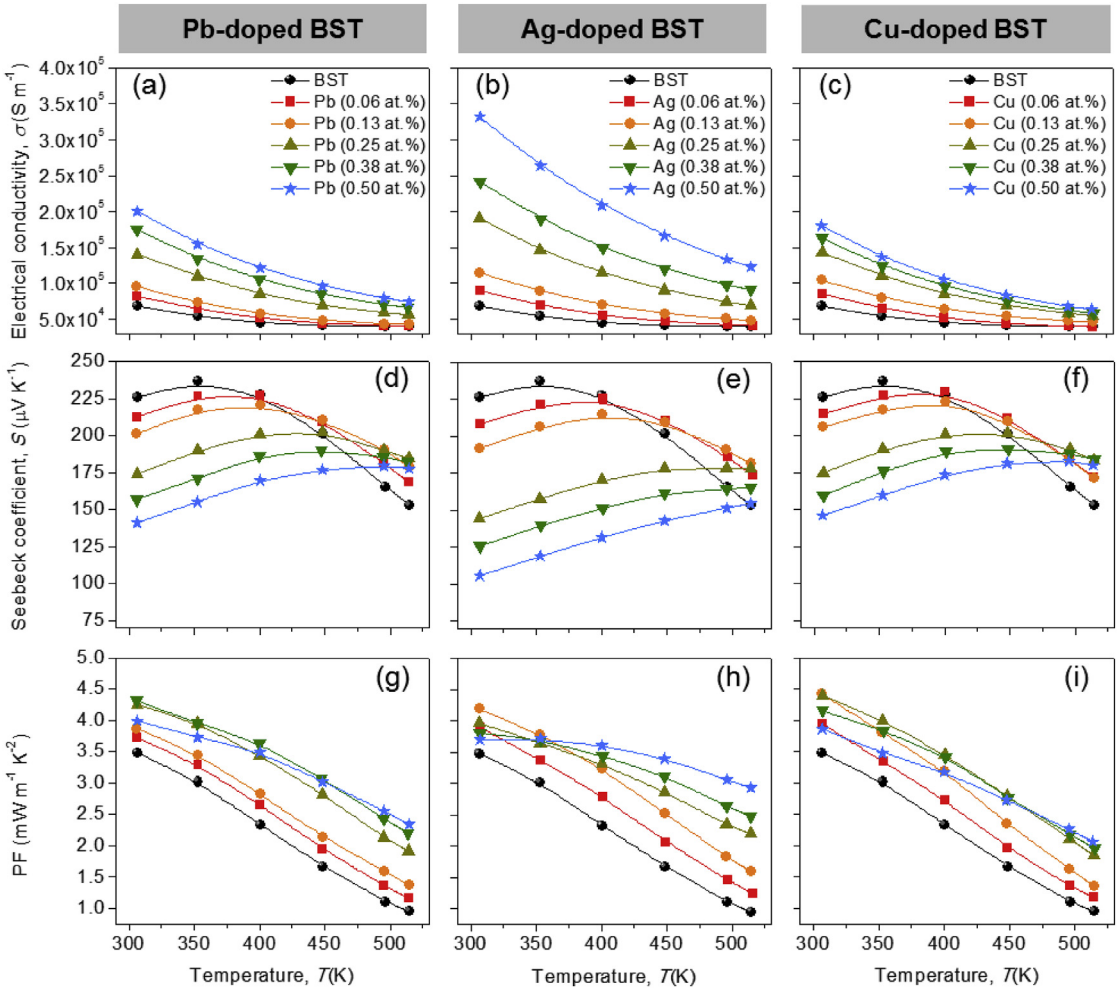

Fig. 2. Temperature dependence of the electrical conductivity of $Bi_{0.52}Sb_{1.48-x}M_xTe_3$ ($x = 0–0.01$(0.5 at.%)), where M is (a) Pb, (b) Ag, and (c) Cu. Temperature dependence of the Seebeck coefficient of $Bi_{0.52}Sb_{1.48-x}M_xTe_3$ ($x = 0–0.01$ (0.5 at.%)), where M is (d) Pb, (e) Ag, and (f) Cu. Temperature dependence of the power factor of $Bi_{0.52}Sb_{1.48-x}M_xTe_3$ ($x = 0–0.01$ (0.5 at.%)), where M is (g) Pb, (h) Ag, and (i) Cu. The data for Pb doping were taken from Ref. [14].

were almost linearly proportional to n_c (Fig. 3(a)). The 0.5 at.% Ag-doped BST sample with the highest n_c of 9.69×10^{19} cm^{-3} showed a μ_{Hall} value (~213 cm^2 V^{-1} s^{-1} at 300 K) comparable to that of undoped BST (~236 cm^2 V^{-1} s^{-1} at 300 K) (Fig. 3(b)). This suggests that the electronic transport properties of BST systems can be tuned to maintain a high power factor by controlling the value of n_c via substitutional doping (Fig. 2(g)–(i)). We also calculated m_d^*, which is another important parameter affecting the power factor of BST systems. It was calculated using the following equation:

$$S = \frac{8\pi^2 k_B^2}{3eh^2}\left(\frac{\pi}{3n_c}\right)^{2/3} m_d^* T, \quad (1)$$

where, k_B, e, and h are the Boltzmann's constant, elementary charge, and Planck's constant, respectively. Fig. 3(c) shows the variation in S with n_c (Pisarenko plot) at 300 and 520 K for $Bi_{0.52}Sb_{1.48-x}M_xTe_3$, The solid lines denote the corresponding m_d^* values for 0.7, 0.9, 1.1, 1.3, and 1.5m_0. We assumed the SPB and energy-independent carrier scattering approximations for degenerated semiconductors. It was found that upon doping, m_d^* increased gradually both at 300 K (0.77m_0 for BST and 1.1m_0 for 0.5 at.% Ag-doped BST) and 520 K (0.83m_0 for BST and 1.66m_0 for 0.5 at.% Ag-doped BST) (inset of Fig. 3(c)). Hence, the enhanced power factor of the doped samples especially at higher temperatures can be attributed to the band engineering effects (such as band flattening and Fermi level tuning) of the samples [11,24]. Fig. 3(d) shows the n_c dependence of the power factor of $Bi_{0.52}Sb_{1.48-x}M_xTe_3$ at 300 and 520 K. At 300 K, a maximum power factor of ~4.4 mW m^{-1} K^{-2} was obtained over the n_c range of 3.0×10^{19}–4.5×10^{19} cm^{-3}, whereas the power factor at 520 K gradually increased from 0.94 mW m^{-1} K^{-2} to 2.93 mW m^{-1} K^{-2} with increase in n_c. This enhancement in the power factor at high temperatures can be attributed to the increased m_d^* and suppressed bipolar conduction at these temperatures.

3.3. Thermal transport properties

The effect of Pb, Ag, and Cu doping on the thermal transport properties of BST were also investigated. Since the thermal transport characteristics of BST are influenced by phonons as well as charge carriers, it is imperative to study their effect separately in order to obtain a clear understanding of the effect of doping. The temperature dependence of κ_{tot} for the $Bi_{0.52}Sb_{1.48-x}M_xTe_3$ samples is shown in Fig. 4(a)–(c). At 300 K, κ_{tot} increased gradually with an increase in the doping content mainly because of the increase in κ_{ele}, as predicted from the σ values. However, at 520 K, the κ_{tot} values of the doped BST samples were lower than that of undoped BST despite their higher σ values. Combined with the enhanced power factor, this unusual feature for the temperature dependent thermal transport could be a decisive factor to shift the

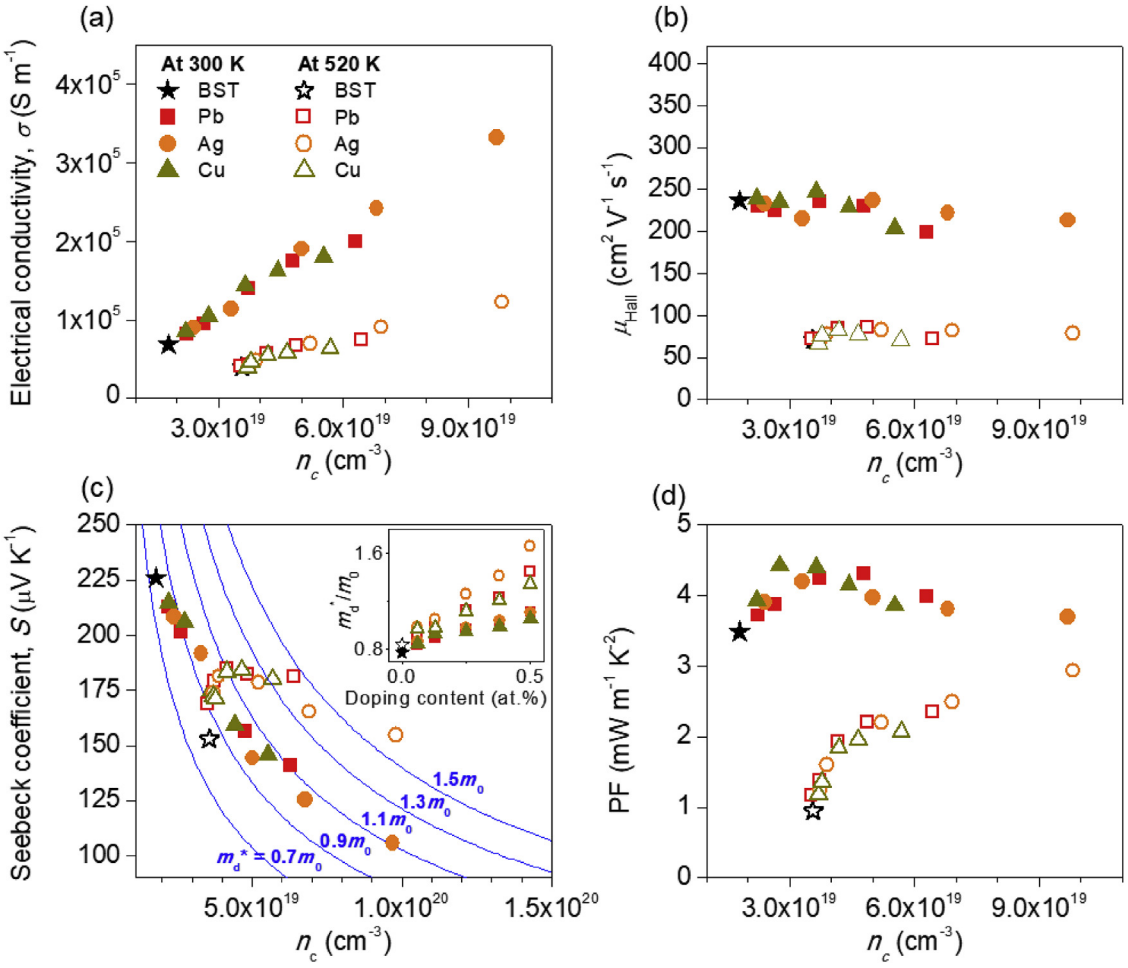

Fig. 3. (a) Electrical conductivity (σ), (b) carrier mobility (μ_{Hall}), (c) Seebeck coefficient (S), and (d) power factor (PF) of $Bi_{0.52}Sb_{1.48-x}M_xTe_3$ ($x = 0$–0.01 (0.5 at.%)), where M is Pb, Ag, and Cu, as a function of the carrier concentration (n_c) at 300 K and 520 K. The inset in (c) shows the m_d^*/m_0 values at 300 and 520 K as a function of the doping content.

temperature for zT_{max} toward higher temperatures as reported in the previous studies [12–20]. We calculated the [κ_{tot} - κ_{ele}] values to clarify this complexity in thermal transport in Bi-Sb-Te systems, and represented them in Fig. 4(d)–(f). The value of κ_{ele} was obtained using the Wiedemann-Franz law ($\kappa_{ele} = L\sigma T$, where L is the Lorenz number). Here, L was estimated using Eq. (2).

$$L = 1.5 + \exp\left[-\frac{|S|}{116}\right], \tag{2}$$

The units of L and S were 10^{-8} W Ω K^{-2} and μV K^{-1}, respectively [25]. The reduced [κ_{tot} - κ_{ele}] values by doping is clearly observed due to the intensified point defect phonon scattering as shown in Fig. 4(g)–(i) especially at 300 K. The unexpected low [κ_{tot} - κ_{ele}] values (<0.4 W m^{-1} K^{-1}) of the 0.38 and 0.5 at.% Ag-doped BST samples can be attributed to the large increase in their σ values, which might cause the larger errors in the calculation of κ_{ele}. Thus, the following theoretical considerations for the thermal transport were carried out except for these two compositions. As is clear from Fig. 4(d)–(f), the inversely proportional relationship between [κ_{tot} - κ_{ele}] and T was not observed, indicating that the [κ_{tot} - κ_{ele}] values could not be directly corresponded to the κ_{lat} values because of the significant bipolar thermal conduction effect. Bipolar conduction was also observed from the temperature-dependence curves of S (Fig. 2(d)–(f)). To further probe the reason for the decrease in κ_{tot} upon doping, κ_{tot} was divided into three distinct components depending on the nature of contribution:

$$\kappa_{tot} = \kappa_{ele} + \kappa_{bp} + \kappa_{lat}, \tag{3}$$

where κ_{lat} is the pure lattice thermal conductivity, and the total electronic contribution is the sum of κ_{ele} andκ_{bp}. The temperature dependence of κ_{bp} and κ_{lat} could be estimated on the basis of the nature of their origin. In general, κ_{bp} is proportional to exp(−1/T) and κ_{lat} is approximately proportional to 1/T. In this study, the κ_{bp} values were calculated based on the two-band and SPB models [21]. Acoustic phonon scattering was also taken into account. In the two-band model, the TE parameters can be obtained using the following equations:

$$\sigma_{tot} = \sigma_p + \sigma_n, \tag{4}$$

$$S_{tot} = \frac{\sigma_p S_p - \sigma_n |S_n|}{\sigma_p + \sigma_n}, \tag{5}$$

$$R_{H_{tot}} = \frac{R_{H_p}\sigma_p^2 + R_{H_n}\sigma_n^2}{(\sigma_p + \sigma_n)^2}, \tag{6}$$

where σ_p, σ_n, S_p, S_n, R_{Hp}, and R_{Hn} are the σ, S, and Hall coefficient for the valence (p) and conduction (n) bands; and σ_{tot} and S_{tot} are the total σ and the total S from the two bands. The σ_{tot} and S_{tot} were fitted to the experimental σ and S by adjusting the deformation

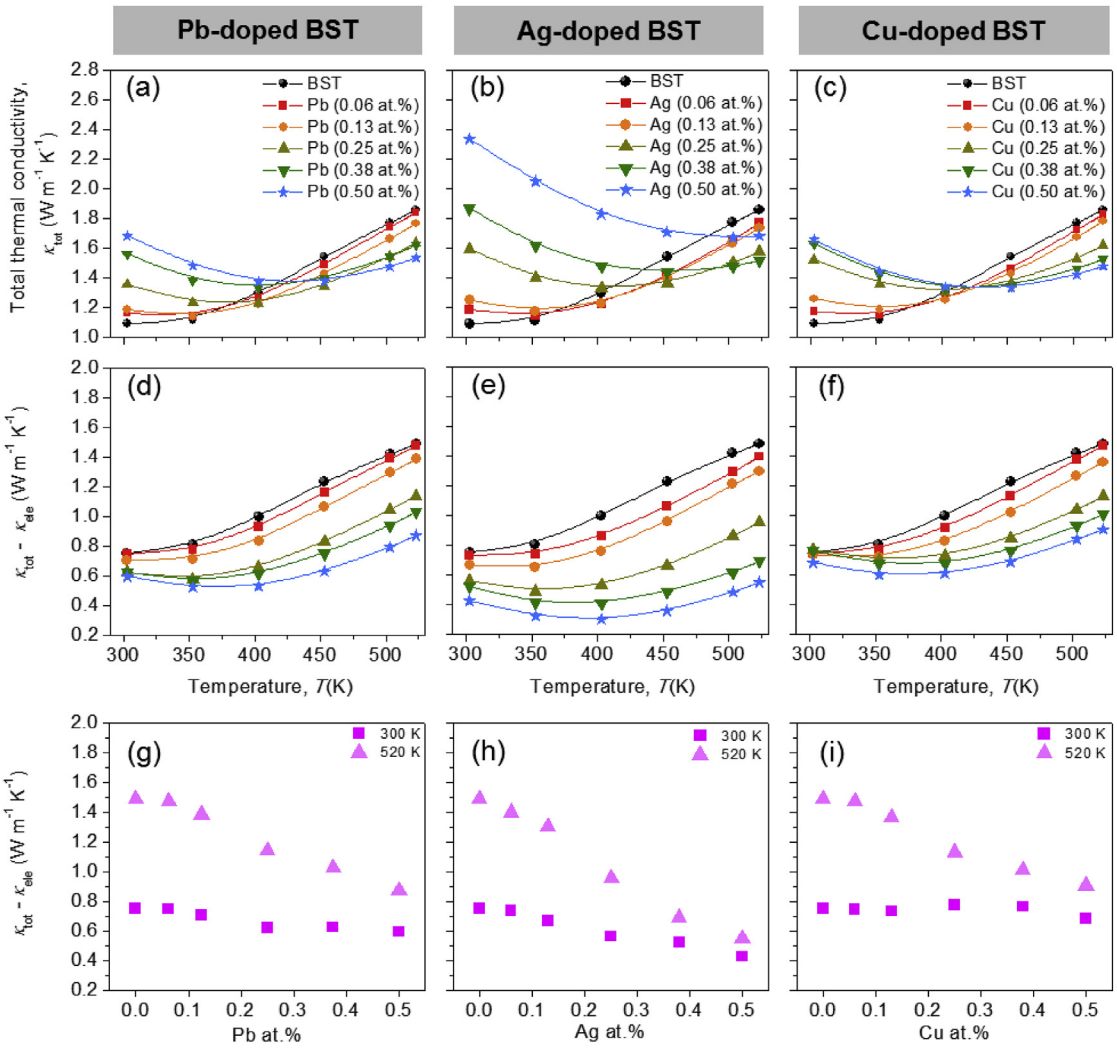

Fig. 4. Temperature dependence of the total thermal conductivity of $Bi_{0.52}Sb_{1.48-x}M_xTe_3$ ($x = 0$–0.01 (0.5 at.%)), where M is (a) Pb, (b) Ag, and (c) Cu. Temperature dependence of the (total − electronic) thermal conductivity of $Bi_{0.52}Sb_{1.48-x}M_xTe_3$ ($x = 0$–0.01(0.5 at.%)), where M is (d) Pb, (e) Ag, and (f) Cu. (g)–(i) The (total − electronic) thermal conductivity of $Bi_{0.52}Sb_{1.48-x}M_xTe_3$ at 300 and 520 K as a function of the doping content. The data for Pb doping were taken from Ref. [14].

potential (E_{def}) and effective mass (m^*) values of the valence (p) and conduction (n) bands. The fitted E_{def} and m^* values of the valence and conduction bands are given in Tables 2–4. Because of the high crystal symmetry of $Bi_xSb_{2-x}Te_3$, the valley degeneracy (N_V) of its highest valence band is 6, while that of the lowest conduction band is 2. The details of the calculation of m^* are given elsewhere [26]. The κ_{bp} value was calculated using the following equation:

$$\kappa_{bp} = \left(S_p^2\sigma_p + S_n^2\sigma_n - S_{tot}^2\sigma_{tot}\right)T \tag{7}$$

The calculated κ_{bp} values of the BST samples are shown in Fig. 5. The contribution of the additional point defect scattering phenomenon induced by doping was analyzed using the Debye-Callaway model [22] while neglecting the contribution of κ_{bp} and κ_{ele}. According to this model

$$\kappa_{lat} = \frac{k_B}{2\pi^2 v}\left(\frac{k_B T}{\hbar}\right)^3 \int_0^{\theta_a/T} \frac{\tau_{tot}(z) z^4 e^z}{(e^z-1)^2} dz, \tag{8}$$

where $\hbar$, θ_a, z, and τ are reduced Planck's constant, Debye temperature, $\hbar\omega/k_BT$, and relaxation time, respectively. The values of θ_a (94 K) [27] and average phonon velocity (2147 m s^{-1}) were obtained from previous reports [28]. The value of κ_{lat} can be calculated using Eq. (8) once the total relaxation time (τ_{tot}) is known. τ_{tot} is the sum of the individual relaxation times (τ_i) for different scattering processes and is given by Eq. (9).

$$\tau_{tot}(z)^{-1} = \sum_i \tau_i(z)^{-1} = \tau_U(z)^{-1} + \tau_B(z)^{-1} + \tau_{PD}(z)^{-1} \tag{9}$$

The individual relaxation times in Eq. (9) correspond to the Umklapp (U), boundary (B), and point-defect (PD) scattering effects. The τ_U and τ_B values were calculated using a previously reported method [26]. The point-defect relaxation time (τ_{PD}) of BST alloys is inversely proportional to the fourth power of the phonon frequency ω and correlates with the fitting parameter (P), which is related to the mass difference and lattice constant difference between the two constituents and the fractional concentration of substitutes (f).

$$\tau_{PD}^{-1} = P f(1-f)\omega^4 \tag{10}$$

The parameter f for the BST alloys ($(Bi_f Sb_{1-f})_2Te_3$) was taken to be 0.26, and P and $Pf(1-f)$ were fitted to 14.55×10^{-41} and

Table 2
Band parameters used to calculate the bipolar thermal conductivity, κ_{bp}, of Pb-doped BST using the two-band model.

Band parameters	$Bi_{0.52}Sb_{1.48}Te_3$	$Bi_{0.52}Sb_{1.48-x}Pb_xTe_3$				
		$x = 0.00125$	$x = 0.0025$	$x = 0.005$	$x = 0.0075$	$x = 0.01$
Valence band (VB) E_{def}[a] (eV)	14.5	13.5	12.9	13.4	13.9	13.8
VB m^* (in m_0)[b]	1.16	1.22	1.28	1.17	1.15	1.19
VB N_V[c]	6	6	6	6	6	6
Conduction band (CB) E_{def}[a] (eV)	9.9	10.3	10.5	9.9	9.3	9
CB m^* (in m_0) [b]	0.83	0.83	0.83	0.83	0.83	0.83
CB N_V[c]	2	2	2	2	2	2
No. of acceptors (10^{19} cm^{-3})	1.80	2.23	2.65	3.71	4.78	6.29
Band gap E_g (eV)	0.15	0.15	0.15	0.15	0.15	0.15
C_l (GPa)[d]	54.7	54.7	54.7	54.7	54.7	54.7

[a] E_{def} = deformation potential.
[b] m^* = effective mass (m_0 = electron mass).
[c] N_V = number of valley degeneracy.
[d] C_l = longitudinal elastic constant.

Table 3
Band parameters used to calculate the bipolar thermal conductivity, κ_{bp}, of Ag-doped BST (except for $x = 0.0075$ and 0.01) using the two-band model.

Band parameters	$Bi_{0.52}Sb_{1.48}Te_3$	$Bi_{0.52}Sb_{1.48-x}Ag_xTe_3$		
		$x = 0.00125$	$x = 0.0025$	$x = 0.005$
Valence band (VB) E_{def}[a] (eV)	14.5	14.1	13.2	14.3
VB m^*(in m_0)[b]	1.16	1.12	1.28	1.09
VB N_V[c]	6	6	6	6
Conduction band (CB) E_{def}[a] (eV)	9.9	9.9	9.4	9.1
CB m^*(in m_0) [b]	0.83	0.83	0.83	0.83
CB N_V[c]	2	2	2	2
No. of acceptors (10^{19} cm^{-3})	1.80	2.41	3.30	5.01
Band gap E_g (eV)	0.15	0.15	0.15	0.15
C_l(GPa)[d]	54.7	54.7	54.7	54.7

[a] E_{def} = deformation potential.
[b] m^* = effective mass (m_0 = electron mass).
[c] N_V = number of valley degeneracy.
[d] C_l = longitudinal elastic constant.

Table 4
Band parameters used to calculate the bipolar thermal conductivity, κ_{bp}, of Cu-doped BST using the two-band model.

Band parameters	$Bi_{0.52}Sb_{1.48}Te_3$	$Bi_{0.52}Sb_{1.48-x}Cu_xTe_3$				
		$x = 0.00125$	$x = 0.0025$	$x = 0.005$	$x = 0.0075$	$x = 0.01$
Valence band (VB) E_{def}[a] (eV)	14.5	13.5	12.9	13.4	13.9	13.8
VB m^*(in m_0)[b]	1.16	1.22	1.28	1.17	1.15	1.19
VB N_V[c]	6	6	6	6	6	6
Conduction band (CB) E_{def}[a] (eV)	9.9	10	10	9.8	9	9.4
CB m^*(in m_0) [b]	0.83	0.83	0.83	0.83	0.83	0.83
CB N_V[c]	2	2	2	2	2	2
No. of acceptors (10^{19} cm^{-3})	1.80	2.23	2.76	3.63	4.42	5.52
Band gap E_g (eV)	0.15	0.15	0.15	0.15	0.15	0.15
C_l(GPa)[d]	54.7	54.7	54.7	54.7	54.7	54.7

[a] E_{def} = deformation potential.
[b] m^* = effective mass (m_0 = electron mass).
[c] N_V = number of valley degeneracy.
[d] C_l = longitudinal elastic constant.

2.80×10^{-41} s^3, respectively. The calculated [$\kappa_{lat} + \kappa_{bp}$] values are denoted by the black solid lines in Fig. 6(a)–(c). For the doped samples, the additional point-defect scattering due to the substitutes was calculated from the separated τ_{PD} parameters using the fractional concentration (f_{doping}) of each substitute in the cation site. For $Bi_{0.52}Sb_{1.48-x}M_xTe_3$ ($x = 0$–0.01, M = Pb, Ag, Cu)), the f_{doping} ($x/2$) values for $x = 0.00125$, 0.0025, 0.005, 0.0075, and 0.01 were 0.000625, 0.00125, 0.0025, 0.00375, and 0.005, respectively. The fitting parameters for the scattering of Pb, Ag, and Cu were fitted to 948.7×10^{-41}(P_{Pb}), 2675×10^{-41}(P_{Ag}), and 761.8×10^{-41} s^3(P_{Cu}), respectively. Therefore, the $P_{doping}f_{doping}(1-f_{doping})$ values for $x = 0.00125$, 0.0025, 0.005, 0.0075, and 0.01 were calculated accordingly (Table 5). In Fig. 6(a)–(c), the calculated values of ($\kappa_{lat} + \kappa_{bp}$) are shown by lines. The P_{doping} parameter was 52–183 times larger than P, accounting for the native cation disorder between Bi and Sb. Therefore, the effect of Pb, Ag, and Cu substitution on κ_{lat} reduction was much greater than that of the native cation disorder. This implies that the interaction of disorders with the matrix (for example bonding nature and structure) is important to induce a strong point-defect scattering effect, which affects the local vibration mode around the point defects. The calculated values of κ_{lat} are represented by solid lines in Fig. 6(d)–(f). Unlike the [κ_{tot}-κ_{ele}] values (Fig. 4(d)–(f)), κ_{lat} was approximately proportional to 1/T by the subtraction of κ_{bp}. It can be clearly observed that

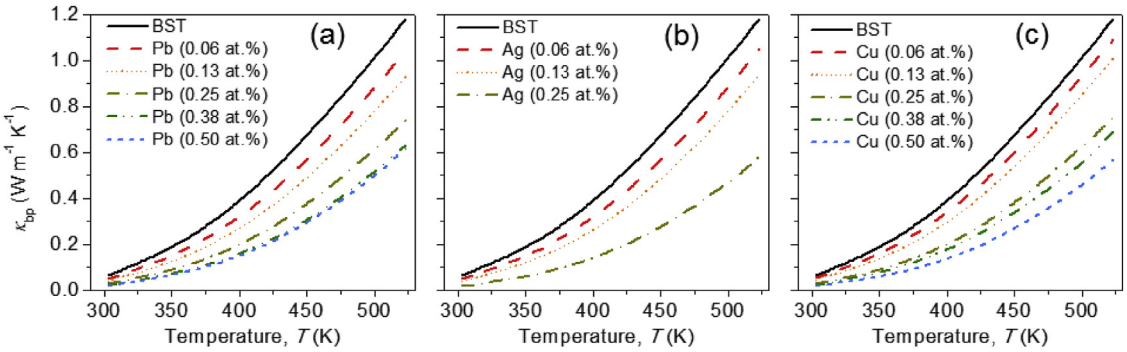

Fig. 5. Temperature dependence of the bipolar thermal conductivity (κ_{bp}) of $Bi_{0.52}Sb_{1.48-x}M_xTe_3$ ($x = 0$–0.01 (0.5 at.%)), where M is (a) Pb, (b) Ag (except for 0.38 at.% and 0.50 at.%), and (c) Cu, as estimated from the two-parabolic band model.

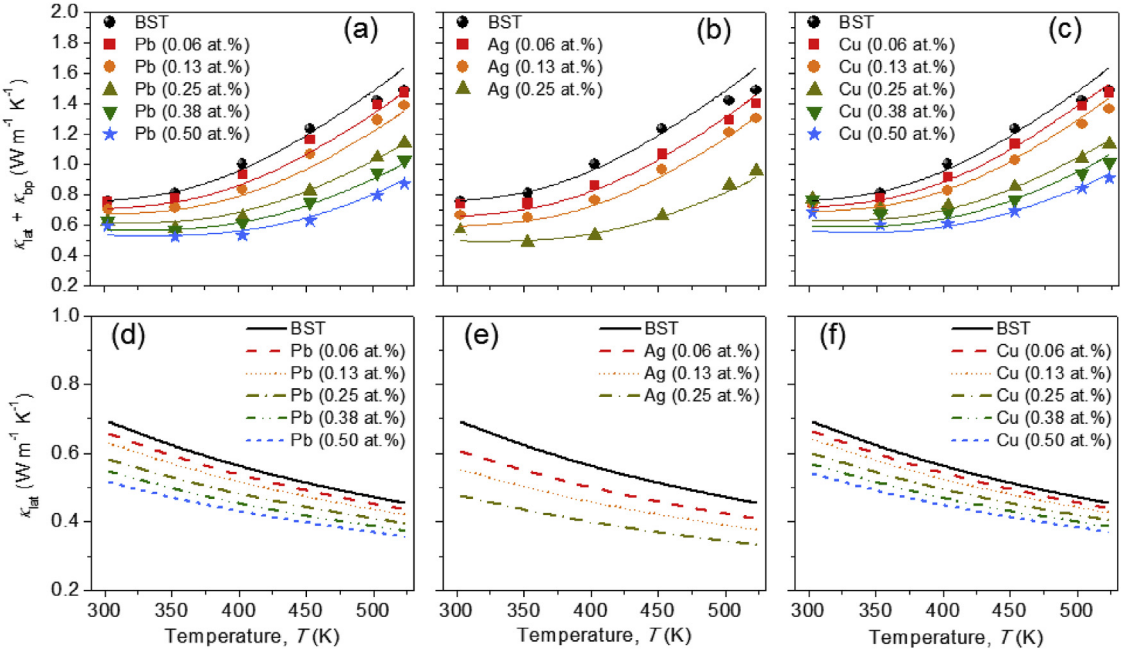

Fig. 6. The ($\kappa_{lat} + \kappa_{bp}$) values of $Bi_{0.52}Sb_{1.48-x}M_xTe_3$ ($x = 0$–0.01 (0.5 at.%)), where M is (a) Pb, (b) Ag (except for 0.38 at.% and 0.50 at.%), and (c) Cu, with fitted values (lines). Temperature dependence of the lattice thermal conductivity (κ_{lat}) of $Bi_{0.52}Sb_{1.48-x}M_xTe_3$ ($x = 0$–0.01 (0.5 at.%)), where M is (d) Pb, (e) Ag (except for 0.38 at.% and 0.50 at.%), and (f) Cu, as estimated from the Debye-Callaway model.

Table 5
The effect of point defect on the total relaxation rate (τ_{total}^{-1}) used to model κ_{lat} of the pristine, Pb-, Ag-(except for $x = 0.0075$ and 0.01), and Cu-doped BST samples.

Sample	τ_{total}^{-1}	Fitting parameter P(10^{-41} s^3)	Fitting parameter P_{Pb} (10^{-41} s^3)	Fitting parameter P_{Ag} (10^{-41} s^3)	Fitting parameter P_{Cu}(10^{-41} s^3)
$Bi_{0.52}Sb_{1.48}Te_3$	$\tau_U^{-1} + \tau_B^{-1} + \tau_{PD}^{-1}$	14.55	948.7	2675	761.8
		P(0.26)(0.74)	**P_{Pb}·f· (1–f)**	**P_{Ag}·f· (1–f)**	**P_{Cu}·f· (1–f)**
$Bi_{0.52}Sb_{1.48-x}M_xTe_3$ $x = 0.00125$ $f = 0.000625$	$\tau_U^{-1} + \tau_B^{-1} + \tau_{PD}^{-1} + \tau_{PD(dopant)}^{-1}$	2.80	0.593	1.67	0.476
$Bi_{0.52}Sb_{1.48-x}M_xTe_3$ $x = 0.0025$ $f = 0.00125$	$\tau_U^{-1} + \tau_B^{-1} + \tau_{PD}^{-1} + \tau_{PD(dopant)}^{-1}$	2.80	1.18	3.34	0.951
$Bi_{0.52}Sb_{1.48-x}M_xTe_3$ $x = 0.005$ $f = 0.0025$	$\tau_U^{-1} + \tau_B^{-1} + \tau_{PD}^{-1} + \tau_{PD(dopant)}^{-1}$	2.80	2.36	6.67	1.90
$Bi_{0.52}Sb_{1.48-x}M_xTe_3$ $x = 0.0075$ $f = 0.00375$	$\tau_U^{-1} + \tau_B^{-1} + \tau_{PD}^{-1} + \tau_{PD(dopant)}^{-1}$	2.80	3.54		2.85
$Bi_{0.52}Sb_{1.48-x}M_xTe_3$ $x = 0.01$ $f = 0.005$	$\tau_U^{-1} + \tau_B^{-1} + \tau_{PD}^{-1} + \tau_{PD(dopant)}^{-1}$	2.80	4.72		3.79

The letters in bold are functions, and the rest are the resulting values.

the κ_{lat} values decreased over the entire temperature range because of the intensified point defect phonon scattering.

The κ_{lat}, κ_{bp}, and κ_{ele} components in the κ_{tot} of pristine and doped (0.25 at.%) BST samples (within the temperature range 300–520 K) are represented by shaded areas in Fig. 7. It can be clearly observed from Fig. 7 that the proportion of κ_{bp} in the BST samples (pristine as well as doped) increased gradually with an increase in temperature. In particular, in pristine BST, κ_{bp} was dominant at higher temperatures. Contrary to pristine BST, the proportions of κ_{bp} to the κ_{tot} values were significantly decreased by doping Pb, Ag, and Cu elements (0.25 at.%), as can be seen from Fig. 7(b)–(d). On the other hand, the proportion of κ_{ele} increased upon doping because of the enhanced σ values of the doped samples. In pristine BST at 520 K, the proportion of κ_{lat}, κ_{bp}, and κ_{ele} in κ_{tot} was 24.3, 63.4, and 12.1%, respectively. These ratios changed to 24.1, 45.1, and 30.7% after Pb doping.

The measured electronic and thermal transport properties of the doped BST alloys were used to calculate their zT values (Fig. 8(a)–(c)). The doped samples showed a zT_{max} value of ~1.15 at temperatures in the range of 350–400 K, which is higher than that

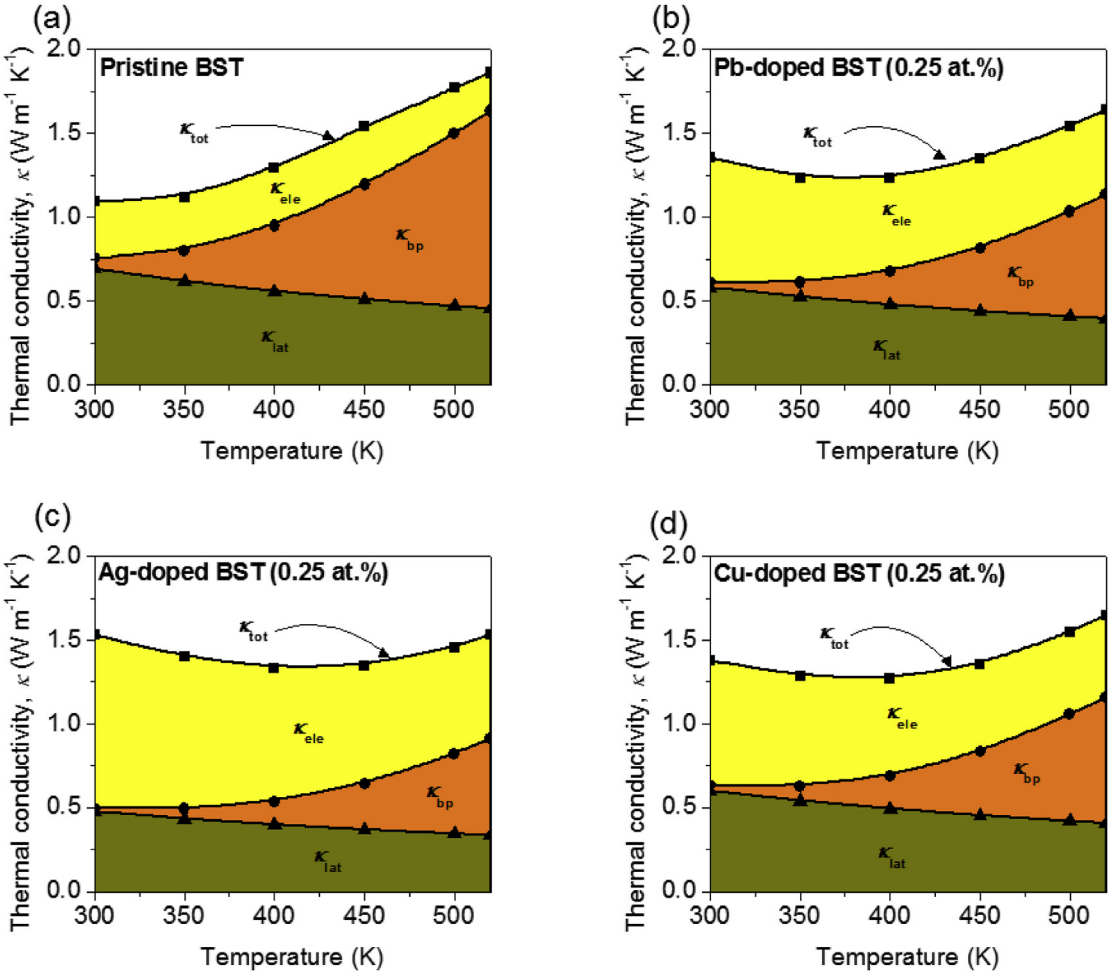

Fig. 7. Thermal conductivities (κ) of (a) pristine BST, (b) 0.25 at.% Pb-doped BST, (c) 0.25 at.% Ag-doped BST, and (d) 0.25 at.% Cu-doped BST. The shaded areas represent the lattice (κ_{lat}), bipolar (κ_{bp}), and electronic (κ_{ele}) thermal conductivity components of κ_{tot}.

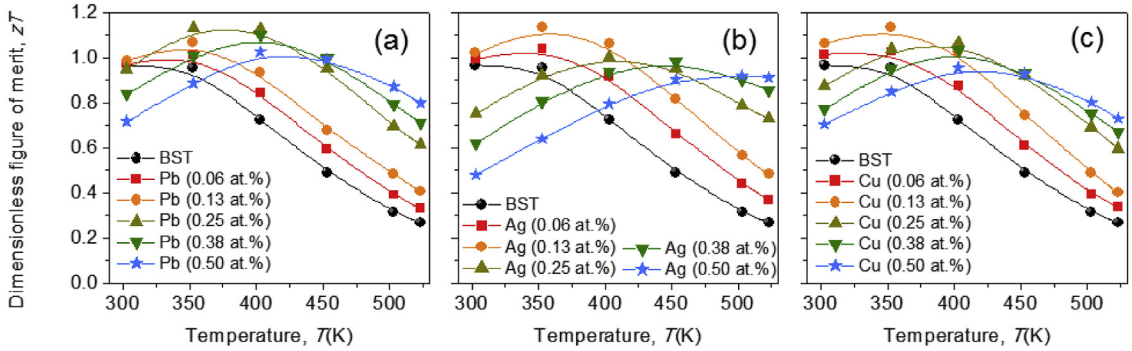

Fig. 8. Dimensionless figure of merit zT of $Bi_{0.52}Sb_{1.48-x}M_xTe_3$ ($x = 0$–0.01 (0.5 at.%)), where M is (a) Pb, (b) Ag, and (c) Cu as a function of temperature. The data for Pb doping were taken from Ref. [14].

obtained for pristine BST (0.95) at 300 K. The enhanced zT values of the doped samples can be attributed to the increase in the power factor and the suppression of κ_{bp} for these samples. However, depending on the doping elements, zT_{max} was obtained at different doping contents: 0.25 at.% for Pb, and 0.13 at.% for Ag and Cu. Unity zT was obtained over the temperature range of 300–400 K because of the suppression of bipolar conduction and the intensified phonon scattering upon optimized doping ($n_c = 2.7–3.7 \times 10^{19}\,cm^{-3}$). In addition, the increased zT values of the samples over the temperature range of 400–520 K improved their TEG efficiency.

4. Conclusions

The electronic and thermal transport properties of systematically designed Pb-, Ag-, and Cu-doped p-type $Bi_{0.52}Sb_{1.48}Te_3$ alloys were measured and analyzed comprehensively in order to understand the mechanism underlying the enhancement of zT by the formation of point defects in p-type BST alloys particularly at temperatures higher than 400 K. Pb, Ag, and Cu doping in the Bi/Sb sites of $Bi_{0.52}Sb_{1.48}Te_3$ effectively generated additional hole carriers, which improved the thermoelectric performance of the alloys especially at higher temperatures mainly because of the suppression of bipolar conduction while maintaining a high carrier mobility. The lattice thermal conductivity of the alloys deceased with an increase in the doping content. This is because the point defect scattering of phonons increased with an increase in the doping content. In addition, doping also modified the band structure (band flattening and Fermi level tuning) of the alloys. At $n_c = 2.7–3.7 \times 10^{19}\,cm^{-3}$, the doped samples showed the maximum zT (~1.15). However, the doping content at which this value was attained depended on the doping element: 0.25 at.% for Pb and 0.13 at.% for Ag and Cu. Hence, $zT > 1$ was obtained over the wide temperature range of 300–400 K, which can contribute to improving the efficiency of low-temperature TEG efficiency of the alloys.

Acknowledgment

This work was supported by the National Research Foundation of Korea (NRF) Grant (2017R1A2A1A17069528) funded by the Korea government (MSIT). KK is grateful for financial support from Yonsei University Research Fund (Post Doc. Researcher Supporting Program) of 2017 (project no.: 2017-12-0039).

References

[1] F.J. DiSalvo, Thermoelectric cooling and power generation, Science 285 (1999) 703.
[2] H.J. Goldsmid, Introduction to Thermoelectricity, second ed., Springer-Verlag Berlin Heidelberg, 2016.
[3] A.S. Rattner, S. Garimella, Energy harvesting, reuse and upgrade to reduce primary energy usage in the USA, Energy 36 (2011) 6172–6183.
[4] S.I. Kim, K.H. Lee, H.A. Mun, H.S. Kim, S.W. Hwang, J.W. Roh, D.J. Yang, W.H. Shin, X.S. Li, Y.H. Lee, G.J. Snyder, S.W. Kim, Dense dislocation arrays embedded in grain boundaries for high-performance bulk thermoelectrics, Science 348 (2015) 109–114.
[5] L. Hu, T. Zhu, X. Liu, X. Zhao, Point defect engineering of high-performance bismuth-telluride-based thermoelectric materials, Adv. Funct. Mater. 24 (2014) 5211–5218.
[6] H. Mun, S.M. Choi, K.H. Lee, S.W. Kim, Boundary engineering for the thermoelectric performance of bulk alloys based on bismuth telluride, ChemSusChem 8 (2015) 2312–2326.
[7] W. Xie, S. Wang, S. Zhu, J. He, X. Tang, Q. Zhang, T.M. Tritt, High performance Bi2Te3 nanocomposites prepared by single-element-melt-spinning spark-plasma sintering, J. Mater. Sci. 48 (2013) 2745–2760.
[8] S. Wang, W. Xie, H. Li, X. Tang, High performance n-type (Bi,Sb)2(Te,Se)3 for low temperature thermoelectric generator, J. Phys. D Appl. Phys. 43 (2010), 335404.
[9] G.J. Snyder, E.S. Toberer, Complex thermoelectric materials, Nat. Mater. 7 (2008) 105–114.
[10] B. Poudel, Q. Hao, Y. Ma, Y. Lan, A. Minnich, B. Yu, X. Yan, D. Wang, A. Muto, D. Vashaee, X. Chen, J. Liu, M.S. Dresselhaus, G. Chen, Z. Ren, High-thermoelectric performance of nanostructured bismuth antimony telluride bulk alloys, Science 320 (2008) 634–638.
[11] G. Tan, L.D. Zhao, M.G. Kanatzidis, Rationally designing high-performance bulk thermoelectric materials, Chem. Rev. 116 (2016) 12123–12149.
[12] B. Xu, M.T. Agne, T. Feng, T.C. Chasapis, X. Ruan, Y. Zhou, H. Zheng, J.H. Bahk, M.G. Kanatzidis, G.J. Snyder, Y. Wu, Nanocomposites from solution-synthesized PbTe-BiSbTe nanoheterostructure with unity figure of merit at low-medium temperatures (500–600 K), Adv. Mater. 29 (2017), 1605140.
[13] C.C. Lin, D. Ginting, R. Lydia, M.H. Lee, J.S. Rhyee, Thermoelectric properties and extremely low lattice thermal conductivity in p-type Bismuth Tellurides by Pb-doping and PbTe precipitation, J. Alloys Compd. 671 (2016) 538–544.
[14] K. Kim, G. Kim, H. Lee, K.H. Lee, W. Lee, Band engineering and tuning thermoelectric transport properties of p-type $Bi_{0.52}Sb_{1.48}Te_3$ by Pb doping for low-temperature power generation, Scripta Mater. 145 (2018) 41–44.
[15] S. Seo, K. Lee, Y. Jeong, M.-W. Oh, B. Yoo, Method of efficient Ag doping for Fermi level tuning of thermoelectric $Bi_{0.5}Sb_{1.5}Te_3$ alloys using a chemical displacement reaction, J. Phys. Chem. C 119 (2015) 18038–18045.
[16] J.K. Lee, S.D. Park, B.S. Kim, M.W. Oh, S.H. Cho, B.K. Min, H.W. Lee, M.H. Kim, Control of thermoelectric properties through the addition of Ag in the $Bi_{0.5}Sb_{1.5}Te_3$ alloy, Electron. Mater. Lett. 6 (2010) 201–207.
[17] J.L. Cui, H.F. Xue, W.J. Xiu, Microstructures and thermoelectric properties of p-type pseudo-binary $Ag_xBi_{0.5}Sb_{1.5-x}Te_3$ (x = 0.05–0.4) alloys prepared by cold pressing, Mater. Lett. 60 (2006) 3669–3672.
[18] Z. Huang, X. Dai, Y. Yu, C. Zhou, F. Zu, Enhanced thermoelectric properties of p-type $Bi_{0.5}Sb_{1.5}Te_3$ bulk alloys by electroless plating with Cu and annealing, Scripta Mater. 118 (2016) 19–23.
[19] Y.S. Lim, M. Song, S. Lee, T.H. An, C. Park, W.S. Seo, Enhanced thermoelectric properties and their controllability in p-type $(BiSb)_2Te_3$ compounds through simultaneous adjustment of charge and thermal transports by Cu incorporation, J. Alloys Compd. 687 (2016) 320–325.
[20] J.L. Cui, H.F. Xue, W.J. Xiu, W. Yang, X.B. Xu, Thermoelectric properties of Cu-doped p-type pseudo-binary $Cu_xBi_{0.5}Sb_{1.5-x}Te_3$ (x=0.05–0.4) alloys prepared by spark plasma sintering, Scripta Mater. 55 (2006) 371–374.
[21] A.F. May, G.J. Snyder, Materials, Preparation, and Characterization in Thermoelectric, CRC Press, Boca Raton, FL, USA, 2012.
[22] J. Callaway, Model for lattice thermal conductivity at low temperatures, Phys. Rev. 113 (1959) 1046–1051.
[23] F.K. Lotgering, Topotactical reactions with ferrimagnetic oxides having hexagonal crystal structures—I, J. Inorg. Nucl. Chem. 9 (1959) 113–123.
[24] Y. Pei, H. Wang, G.J. Snyder, Band engineering of thermoelectric materials, Adv. Mater. 24 (2012) 6125–6135.
[25] H.S. Kim, Z.M. Gibbs, Y. Tang, H. Wang, G.J. Snyder, Characterization of Lorenz number with Seebeck coefficient measurement, Apl. Mater. 3 (2015), 041506.
[26] H. Kim, S.I. Kim, K.H. Lee, S.W. Kim, G.J. Snyder, Phonon scattering by dislocations at grain boundaries in polycrystalline $Bi_{0.5}Sb_{1.5}Te_3$, Phys. Status Solidi B 254 (2017), 1600103.
[27] D. Bessas, I. Sergueev, H.C. Wille, J. Perßon, D. Ebling, R.P. Hermann, Lattice dynamics in Bi_2Te_3 and Sb_2Te_3: Te and Sb density of phonon states, Phys. Rev. B 86 (2012), 224301.
[28] F. Yang, T. Ikeda, G.J. Snyder, C. Dames, Effective thermal conductivity of polycrystalline materials with randomly oriented superlattice grains, J. Appl. Phys. 108 (2010), 034310.